Gauge-invariant real-space method for density functional calculations in an external magnetic field

S. Janecek and E. Krotscheck
Institut für Theoretische Physik, Johannes Kepler Universität, A 4040 Linz, Austria
(Received 29 February 2008; published 16 June 2008)

This paper describes a configuration-space method for *ab initio* electronic structure calculations in an arbitrarily strong external magnetic field. Special attention is paid to a manifestly gauge-invariant formulation of the problem that is independent of the discretization. We will show that rigorous gauge invariance can be implemented quite efficiently in real-space methods. To be able to reproduce empirical data for realistic systems, we also formulate our real-space algorithm in magnetic fields for nonlocal ionic pseudopotentials. Here, gauge invariance is again an issue, but has to be maintained by construction of such potentials. Numerical applications focus on two points. The first one is a careful assessment of the convergence properties of our algorithm and in particular the implications of our gauge-invariant formulation. We then calculate the magnetic susceptibilities and nuclear magnetic resonance shifts for a number of typical molecules of physical interest and compare with previous work.

DOI: 10.1103/PhysRevB.77.245115 PACS number(s): 31.15.E−, 33.15.Kr, 33.25.+k

I. INTRODUCTION

We report here on further developments of our real-space method[1–3] for solving Schrödinger-like equations as, for example, the Kohn–Sham[4,5] equations of density functional theory (DFT), in two or three dimensions and arbitrary geometries. We have recently shown[6,7] how local one-body Schrödinger equations can be solved in real space for strong uniform magnetic fields with—apart from the fact that all orbitals are complex—practically no computational overhead compared to the field-free case. The method was applied in two dimensions for quantum dots in strong magnetic fields.[7] Due to the efficiency of the method, we were able to study the statistics of tens of thousands of configurations.

The present paper is specifically concerned with an implementation for arbitrarily strong, uniform magnetic fields in three dimensions that is gauge-invariant independent of the discretization. This extension is motivated, among others, by recent experimental prospects to reach field strengths of up to 100 T. Interesting physical effects are found in the band structure of materials, conduction properties of rare-earth metals, and organic magnets. Literature on these topics is abundant, see Refs. 8–11 for just a few examples. We stress, however, that the method also provides improvements over previous work in the regime of linear magnetic response.

An important aspect connected with magnetic fields is the gauge invariance of the method. The problem of the gauge invariance of "*ab initio*" theories has two aspects: The first has to do with the fact that the Schrödinger equation must be approximated by a discrete representation in a finite basis, a process that usually destroys gauge invariance. In quantum chemistry the term "gauge origin problem" has been coined for this aspect. The problem has been discussed at length in the literature, see, for example, the review by Helgaker, Jaźuński and Ruud.[12] These authors state explicitly that *within a finite linear variational subspace, gauge invariance can never be obtained exactly, only approximately for small displacements of the gauge origin.*

The second aspect has to do with the fact that local Hamiltonians are in most cases insufficient to reproduce the properties of realistic molecules and clusters. Therefore, nonlocal "pseudopotentials" have been introduced; the gauge-invariant construction of such pseudopotentials is an entirely different issue; we will get back to this point later.

Several methods to deal with the gauge origin problem have been discussed. The conventional method (CONV) (Refs. 13 and 14) basically ignores the problem and uses a single gauge origin centered at the charge centroid of the molecule. An improvement is the "individual gauge for localized orbitals" (IGLO) method,[15,16] where the gauges of the final wave functions are transformed to their centers of charge. The individual gauges for atoms in molecules (IGAIM) (Ref. 17) method uses atom-centered gauge origins for calculating the current density inside the "basin" of a single atom, while the continuous set of gauge transformations (CSGT) (Ref. 18) method uses a different gauge for each position where the induced current is to be calculated. Sebastiani[19] has derived a variant of CSGT that is suitable for periodic systems. The Mauri–Pfrommer–Louie (MPL) method[20] has also been designed for calculating magnetic response properties of systems subject to periodic boundary conditions. It is based on a spatially modulated magnetic field, the experimental situation of infinite modulation wavelength is extrapolated numerically.

Our main concern here is to formulate the diffusion algorithm for *local* Hamiltonians on a discrete mesh in coordinate space in a way that is gauge-invariant *independent of the discretization.* This is done in Secs. II B and II C. We will show that gauge invariance can be achieved without any additional computational effort. This is a distinctive feature of real-space and plane-wave formulations of the problem.

The second aspect needed for the calculation of properties of most realistic molecules and clusters is, of course, a way to deal with nonlocal pseudopotentials. We have recently formulated the real-space diffusion algorithm for nonlocal potentials of the Kleinman–Bylander type[21] in zero magnetic field,[3] we extend the method here to uniform external magnetic fields. The problem of gauge invariance surfaces again, but at a different level because gauge invariance has to be a

construction objective of such pseudopotentials. Here we will essentially follow the work of Pickard and Mauri[22] to define gauge-invariant pseudopotentials, and only briefly mention aspects of this question that are relevant to the convergence of our real-space diffusion algorithm.

Our paper is organized as follows: In Sec. II we describe the real-space algorithm for simple local pseudopotentials in detail. We will spell out a specific family of representations of the kinetic-energy operator that maintains gauge invariance in any discretization. We then generalize the method to realistic nonlocal pseudopotentials of the Kleinman–Bylander type and discuss to what extent an external magnetic field can affect the convergence properties.

As a first set of numerical applications, we demonstrate the efficiency of the fourth order factorization of the diffusion operator—compared to second-order methods—by studying the three-dimensional Fock–Darwin model. We demonstrate numerically the gauge invariance of our method and highlight the errors induced by naïve, non-gauge-invariant discretizations. We then apply the method to a C_6H_6 molecule and show that the presence of a magnetic field does not affect convergence rate up to unreasonably high magnetic-field strengths. We also demonstrate the gauge invariance of our algorithm and compare with the errors induced by non-gauge-invariant discretizations.

We finally apply the algorithm for calculating the electronic structure, magnetic susceptibility and nuclear-magnetic-resonance (NMR) shieldings for a representative set of molecules and find agreement with experimental results and previous work within the expected accuracy.

II. REAL SPACE DIFFUSION ALGORITHM FOR SOLVING SCHRÖDINGER EQUATIONS IN A UNIFORM MAGNETIC FIELD

A. Diffusion algorithm

The numerical solution of single-particle Schrödinger-type equations is central to many problems in computational quantum mechanics. Among others, the Kohn–Sham equations of density functional theory are of the form

$$\hat{H}\psi_j(\mathbf{r}) = E_j\psi_j(\mathbf{r}), \tag{2.1}$$

where $\hat{H}$ is typically of the form

$$\hat{H} = \hat{T} + \hat{V} \tag{2.2}$$

with a one-body kinetic-energy operator $\hat{T}$ and a (local or nonlocal) potential energy $\hat{V}$.

A fast and conceptually simple method for calculating the lowest n solutions of the one–body Schrödinger equation is the diffusion algorithm. The strategy is to apply the evolution operator in imaginary time,

$$\mathcal{T}(\epsilon) \equiv e^{-\epsilon\hat{H}}, \tag{2.3}$$

repeatedly to a set of states $\{\psi_j(\mathbf{r}), 1 \le j \le n\}$, and to orthogonalize the states after every step. This procedure converges toward the lowest n eigensolutions of the Hamiltonian $\hat{H}$.

The evolution operator [Eq. (2.3)] cannot be calculated exactly for a Hamiltonian of the form (2.2), it has to be approximated, e.g., by factorization formulas. A well-known second-order factorization of the evolution operator corresponding to the Hamiltonian (2.2) is the Trotter formula

$$\mathcal{T}(\epsilon) \equiv e^{-\epsilon(\hat{T}+\hat{V})} = e^{-(1/2)\epsilon\hat{V}}e^{-\epsilon\hat{T}}e^{-(1/2)\epsilon\hat{V}} + \mathcal{O}(\epsilon^3). \tag{2.4}$$

Factorizing $\mathcal{T}(\epsilon)$ reduces the problem of calculating the exponential of the Hamiltonian to the problem of dealing with the different factors separately. If $\hat{T}$ is a local operator in momentum space, and $\hat{V}$ is local in coordinate space, then calculating $e^{-(1/2)\epsilon\hat{V}}\psi$ and $e^{-\epsilon\hat{T}}\psi$ is almost trivial.

The above factorization of the exact evolution operator corresponds to approximating the Hamiltonian, the converged solutions obtained by the method are therefore functions of the time step ϵ. The smaller the time step, the more accurate is the solution, but on the other hand, the algorithm converges faster when the time step is large. It is therefore desirable to use factorizations of higher order in ϵ to achieve the same accuracy with less computational effort.

In the last decade, fourth order forward factorization schemes have become available for solving imaginary time evolution equations.[23–25] These include the operator $[\hat{V},[\hat{T},\hat{V}]]$, which is just another (local) potential. We have recently demonstrated[1,2] for local Hamiltonians that these fourth order forward factorizations lead to very rapid convergence for realistic systems at large time steps and therefore provide a powerful method for solving typical problems in density functional theory. A specific fourth–order factorization is[24,26]

$$\mathcal{T}^{(4)}(\epsilon) \equiv e^{-(1/6)\epsilon\hat{V}}e^{-(1/2)\epsilon\hat{T}}e^{-(2/3)\epsilon\hat{D}}e^{-(1/2)\epsilon\hat{T}}e^{-(1/6)\epsilon\hat{V}} = \mathcal{T}(\epsilon) + \mathcal{O}(\epsilon^5) \tag{2.5}$$

where

$$\hat{D} = \hat{V} + \frac{1}{48}\epsilon^2[\hat{V},[\hat{T},\hat{V}]]. \tag{2.6}$$

The method is particularly simple for local potentials, $\hat{V} = V(\mathbf{r})$, because the double commutator

$$[\hat{V},[\hat{T},\hat{V}]](\mathbf{r}) = \frac{\hbar^2}{m}|\nabla V(\mathbf{r})|^2 \tag{2.7}$$

is just another local potential. Thus, the core of the algorithm is quite simple and can be implemented using readily available library routines.[27]

B. Uniform magnetic fields

We have so far not specified the kinetic-energy operator $\hat{T}$. In the presence of a vector potential $\mathbf{A}(\mathbf{r})$, the momentum operator $\mathbf{p} = -i\hbar\nabla$ is replaced by the canonical momentum operator

$$\Pi = -i\hbar\nabla + e\mathbf{A}_{\text{ext}}(\mathbf{r}), \tag{2.8}$$

and the kinetic-energy operator is

$$\hat{T} = \frac{1}{2m}[-i\hbar\nabla + e\mathbf{A}_{\text{ext}}(\mathbf{r})]^2 = \frac{1}{2m}[\Pi_x^2 + \Pi_y^2 + \Pi_z^2]. \tag{2.9}$$

The key to the inclusion of a uniform and arbitrarily strong magnetic field is the evaluation of the exponential of the *canonical* kinetic-energy operator [Eq. (2.9)]. To be specific, we assume that the magnetic field is in z direction. It is computationally most efficient to work in linear gauge

$$\mathbf{A}(\mathbf{r}) = -By\mathbf{e}_x. \tag{2.10}$$

In analogy to the harmonic oscillator,[28] the density matrix $e^{-\epsilon\hat{T}}$ can be calculated exactly:

$$e^{-(\epsilon/2m)(\Pi_x^2+\Pi_y^2+\Pi_z^2)} = e^{-(\epsilon/2m)C_x(\xi)\Pi_x^2}e^{-(\epsilon/2m)C_y(\xi)\Pi_y^2}e^{-(\epsilon/2m)C_x(\xi)\Pi_x^2}e^{-(\epsilon/2m)\Pi_z^2}, \tag{2.11}$$

where $\xi = \epsilon\hbar eB/m$, and

$$C_x(\xi) = \frac{\cosh(\xi) - 1}{\xi\sinh(\xi)} \quad \text{and} \quad C_y(\xi) = \frac{\sinh(\xi)}{\xi}. \tag{2.12}$$

The z component factorizes trivially due to

$$[\Pi_x, \Pi_z] = [\Pi_y, \Pi_z] = 0. \tag{2.13}$$

C. Gauge invariance

A *gauge transformation*, i.e., adding a gradient to the vector potential

$$\boldsymbol{A}(\mathbf{r}) \to \boldsymbol{A}'(\mathbf{r}) = \boldsymbol{A}(\mathbf{r}) + \nabla\chi(\mathbf{r}) \tag{2.14}$$

does not change the magnetic field $\mathbf{B} = \nabla \times \mathbf{A}$. Under the gauge transformation, the wave functions simply acquire a phase factor[29]

$$\psi(\mathbf{r}) \to \psi'(\mathbf{r}) = e^{-i(e/\hbar)\chi(\mathbf{r})}\psi(\mathbf{r}). \tag{2.15}$$

Defining

$$f_j(\mathbf{r}) \equiv \int_{x_j} A_j(\mathbf{r})dx_j, \tag{2.16}$$

we can write the action of the j^{th} component of the canonical momentum operator [Eq. (2.8)] on a wave function as

$$\Pi_j\psi(\mathbf{r}) = -i\hbar\left[\frac{\partial}{\partial x_j} + \frac{ie}{\hbar}A_j(\mathbf{r})\right]\psi(\mathbf{r}) = e^{-i(e/\hbar)f_j(\mathbf{r})}\left[-i\hbar\frac{\partial}{\partial x_j}\right]e^{+i(e/\hbar)f_j(\mathbf{r})}\psi(\mathbf{r}). \tag{2.17}$$

The operation (2.17) is known as *covariant derivative*.[30] For the square of this operator, evidently

$$\Pi_j^2\psi(\mathbf{r}) = -\hbar^2\left[\frac{\partial}{\partial x_j} + i\frac{e}{\hbar}A_j(\mathbf{r})\right]^2\psi(\mathbf{r}) = -\hbar^2 e^{-i(e/\hbar)f_j(\mathbf{r})}\frac{\partial^2}{\partial x_j^2}e^{+i(e/\hbar)f_j(\mathbf{r})}\psi(\mathbf{r}) \tag{2.18}$$

holds. We can therefore cast the canonical kinetic-energy operator in the form

$$\frac{1}{2m}\Pi^2 = -\frac{\hbar^2}{2m}\sum_j e^{-i(e/\hbar)f_j(\mathbf{r})}\frac{\partial^2}{\partial x_j^2}e^{i(e/\hbar)f_j(\mathbf{r})}. \tag{2.19}$$

A gauge transformation [Eq. (2.14)] simply transforms the functions $f_j(\mathbf{r})$ as

$$f_j(\mathbf{r}) \to f_j'(\mathbf{r}) = f_j(\mathbf{r}) + \chi(\mathbf{r}), \tag{2.20}$$

and in turn the canonical momentum operator transforms as

$$\frac{1}{2m}\Pi^2 \to \frac{1}{2m}\Pi'^2 = \frac{1}{2m}e^{-i(e/\hbar)\chi(\mathbf{r})}\Pi^2 e^{+i(e/\hbar)\chi(\mathbf{r})}. \tag{2.21}$$

In the following, we will refer to operators having the property (2.21) as "gauge-invariant operators." If the potential operator is also gauge invariant, which is trivially true for local potentials, the whole Hamiltonian is, and the Schrödinger equation transforms as

$$\hat{H}\psi_j(\mathbf{r}) = E_j\psi_j(\mathbf{r}) \to e^{-i(e/\hbar)\chi(\mathbf{r})}\hat{H}e^{+i(e/\hbar)\chi(\mathbf{r})}\psi_j'(\mathbf{r}) = e^{-i(e/\hbar)\chi(\mathbf{r})}E_j'e^{+i(e/\hbar)\chi(\mathbf{r})}\psi_j'(\mathbf{r}). \tag{2.22}$$

Consequently, $E_j' = E_j$, and the wave function transforms according to Eq. (2.15).

In numerical real-space calculations, the wave function is represented on a discrete mesh. For a function $f(x)$ defined on a finite grid $\{x_i\}$, the $(2n+1)$-point finite-difference approximations of $df(x)/dx|_{x=x_i}$ and $d^2f(x)/dx^2|_{x=x_i}$ are

$$\left[\frac{d}{dx}f\right]_n(x_j) \equiv \frac{1}{2h}\sum_{m=-n}^{+n} b_m^{(1)}f(x_{j+m}), \quad \text{with} \quad b_m^{(1)} = -b_{-m}^{(1)} \tag{2.23}$$

$$\left[\frac{d^2}{dx^2}f\right]_n(x_j) \equiv \frac{1}{h^2}\sum_{m=-n}^{+n} b_m^{(2)}f(x_{j+m}), \quad \text{with} \quad b_m^{(2)} = b_{-m}^{(2)}, \tag{2.24}$$

where h is the distance between the mesh points, and the coefficients $b_m^{(1)}$ and $b_m^{(2)}$ are determined by differentiating a $(2n+1)$-point Lagrange interpolating polynomial. Recurrence relations for the coefficients are, e.g., given by Dvornikov,[31] see also Ref. 32.

The chain- and product-rules, which are needed to go from the second to the third expression in Eq. (2.17), are not exactly satisfied by finite-difference operators. Thus, if one naïvely uses formulas (2.23) or (2.24) in a discrete representation of the canonical kinetic-energy operator [Eq. (2.9)], gauge invariance will normally be destroyed. This is, in practical applications, an important aspect: In three dimensions, it is crucial to use a grid that is as coarse as possible in order to keep the computational effort affordable. The problem is

cured by simply using the representation (2.19) for the kinetic energy. Then

(i) In the continuum limit, i.e., the limit of an infinitely fine discretization $h \to 0$, the difference between the solutions of the discretized and the continuum Schrödinger equation vanishes.

(ii) In any finite discretization of the Laplacian, the canonical momentum operator retains the gauge invariance property [Eq. (2.21)] by construction.

Of course, to be applicable in the diffusion algorithm, it must be possible to calculate the exponential of the full canonical kinetic-energy operator. This is always approximately feasible for *general* magnetic fields by using the Baker–Campbell–Hausdorff formula for the three components. However, for a *homogeneous* magnetic field, the exact formula (2.11) provides a much more elegant solution.

The action of the kinetic-energy operator on a wave function can be calculated very efficiently in Fourier space. Plane waves are the eigenfunctions of the Laplacian in *any* discretization,

$$\left[-\hbar^2 \frac{d^2}{dx^2} e^{ikx}\right]_n (x_j) = \left(-\frac{\hbar^2}{h^2} \sum_{m=-n}^{n} b_m^{(2)} e^{ikmh}\right) e^{ikx_j} \equiv t_n(k) e^{ikx_j}. \tag{2.25}$$

The eigenvalues $t_n(k)$ can be calculated exactly (correcting Eq. (52) in Ref. 2),

$$t_n(k) = \hbar^2 k^2 \frac{\sin^2 \xi}{\xi^2}\left[1 + \frac{1}{3}\sin^2 \xi + \frac{8}{45}\sin^4 \xi + \frac{4}{35}\sin^6 \xi + \frac{128}{1575}\sin^8 \xi + \ldots\right], \tag{2.26}$$

where $\xi = hk/2$, and the terms in the square bracket consecutively refer to a 3, 5, 7, 9, …—point formula for the second derivative. The same is of course also true for the first derivatives, where we define

$$\left[-i\hbar \frac{d}{dx} e^{ikx}\right]_n (x_j) \equiv p_n(k) e^{ikx_j}. \tag{2.27}$$

Expanding, e.g., the x component of the wave function in plane waves,

$$\psi(x,y,z) = \sum_{k_x} \tilde{\psi}(k_x,y,z) e^{ik_x x},$$

the action of the operator [Eq. (2.23)] on $\psi(x,y,z)$ can be efficiently calculated in Fourier space,

$$\left[-\hbar^2 \frac{d^2}{dx^2}\psi\right]_n (x_j,y,z) = \sum_{k_x} \tilde{\psi}(k_x,y,z) t_n(k_x) e^{ik_x x_j}. \tag{2.28}$$

For specific forms of the vector potential, this relationship can also be utilized for the components of the canonical momentum operator. If the j^{th} component of the vector potential does not depend on x_j, the function f_j is linear in x_j, e.g., for the x component

$$f_x(x,y,z) = xA_x(y,z). \tag{2.29}$$

In homogeneous fields, this is the case, e.g., for symmetric and linear gauge. In linear gauge, for a magnetic field in z-direction, we have [cf. Eq. (2.10)]

$$f_x(\mathbf{r}) = Bxy, \quad f_y(\mathbf{r}) = f_z(\mathbf{r}) = 0. \tag{2.30}$$

Again expanding $\psi(\mathbf{r})$ in-plane waves, we have

$$e^{i(e/\hbar)f_x(\mathbf{r})}\psi(x,y,z) = \sum_{k_x} \tilde{\psi}(k_x,y,z) e^{ix(k_x + (e/\hbar)A_x(y,z))}, \tag{2.31}$$

and thus

$$\Pi_x^2 \psi(x_j,y,z) = e^{-i(e/\hbar)f_x(x_j,y,z)}\left[-\hbar^2 \frac{d^2}{dx^2} e^{+i(e/\hbar)f_x}\psi\right]_n (x_j,y,z) \tag{2.32}$$

$$= \sum_{k_x} \tilde{\psi}(k_x,y,z) t_n\left(k_x + \frac{e}{\hbar}A_x(y,z)\right) e^{ik_x x_j}. \tag{2.33}$$

Consequently, calculating the action of the canonical momentum operator is no more complicated than calculating the action of the ordinary momentum operator, its eigenvalues are simply shifted by $eA_x(y,z)/\hbar$. Therefore, the calculation of the exponential of the kinetic-energy operator (2.11) is, in momentum space, also trivial. In particular, rigorous gauge invariance is maintained in any discretization without additional effort.

The action of the kinetic-energy part of the evolution operator in a uniform magnetic field [Eq. (2.10)] on an arbitrary wave function is then computed as follows:

(1) Fourier transform, for all y, the x and the z coordinates of each state to (k_x,y,k_z) space and multiply by $e^{-(\epsilon/2m)[C_x(\epsilon)\Pi_x^2 + \hbar^2 k_z^2]} = e^{-(\epsilon/2m)[C_x(\epsilon)t_n(k_x + By/\hbar) + t_n(k_z)]}$.

(2) Fourier transform now the y coordinate to k_y space, and multiply by $e^{-(\epsilon/2m)C_y(\epsilon)t_n(k_y)}$.

(3) Do the inverse transformation back to (k_x,y,k_z) and multiply by $e^{-(\epsilon/2m)C_x(\epsilon)t_n(k_x + eBy/\hbar)}$.

(4) Fourier transform k_x and k_z back to coordinate space.

Thus, in a cubic grid of N^3 points, the propagation with the kinetic-energy operator takes $2N$ two-dimensional and $2N^2$ one-dimensional Fourier transforms, which is equivalent to two three-dimensional transforms that are needed for the propagation of the normal kinetic-energy operator without a magnetic field. Computational overhead is only caused by the fact that all wave functions are complex.

While it is not the subject of this paper, we should stress that our method is not restricted to homogeneous magnetic fields. First, because of the form [Eq. (2.18)] of the components of the kinetic energy, we also have

$$e^{-(\epsilon/2m)\Pi_j^2}\psi(\mathbf{r}) = e^{-i(\epsilon/\hbar)e f_j(\mathbf{r})} e^{(\epsilon\hbar^2/2m)(\partial^2/\partial x_j^2)} e^{+i(e/\hbar)f_j(\mathbf{r})}\psi(\mathbf{r}). \tag{2.34}$$

Thus, while abandoning an *exact* calculation of $e^{-\epsilon\hat{T}}$ for nonuniform magnetic fields, we can use at least standard second-order factorization techniques to calculate this operator. This would destroy rigorous fourth order convergence, the use of

the factorization [Eq. (2.5)] should still be advantageous over Eq. (2.4) because the effects of a magnetic field are expected to be small in most realistic cases.

D. Nonlocal potentials

Quantitatively accurate electronic structure calculations for realistic systems can normally not be obtained by describing the ion cores by local potentials. We have in recent work[3] generalized the above evolution operator scheme for DFT calculations combined with nonlocal pseudopotentials. In that case, the potential consists of two noncommuting terms and the Hamiltonian consists of three noncommuting terms:

$$\hat{V} = \hat{V}_{\rm loc} + \hat{V}_{nl}, \quad \hat{H} = \hat{T} + \hat{V}_{\rm loc} + \hat{V}_{nl} \equiv \hat{H}_{\rm loc} + \hat{V}_{nl}, \tag{2.35}$$

where $\hat{V}_{\rm loc}$ gathers all local contributions to the potential (Hartree, exchange correlation and local part of the pseudopotentials in case of density functional theory), while $\hat{V}_{nl}$ represents the nonlocal part of the pseudopotentials used to describe the interaction of the valence electrons with the ion cores. A popular choice for V_{nl} is the Kleinman–Bylander[21] separable form: The nonlocal part of the Hamiltonian has the structure

$$\begin{aligned} V_{\rm nl}(\mathbf{r},\mathbf{r}') &= \sum_{i=1}^{N} v_{\rm nl}^{(i)}(\mathbf{r}-\mathbf{R}_i,\mathbf{r}'-\mathbf{R}_i) \\ &= \sum_{i=1}^{N}\sum_{m} A_\ell^{(i)} \langle \mathbf{r}-\mathbf{R}_i \,|P_{\ell m}^{(i)}\rangle\langle P_{\ell m}^{(i)}|\, \mathbf{r}'-\mathbf{R}_i\rangle. \end{aligned} \tag{2.36}$$

In the above equation, $A_\ell^{(i)}$ are numerical constants characterizing the pseudopotential, the $P_{\ell m}^{(i)}$ are functions defined as $P_{\ell m}^{(i)}=R_\ell^{(i)}(r)Y_{\ell m}$, where $R_\ell(r)$ is a radial function, and $Y_{\ell m}$ are spherical harmonics. The $\mathbf{R}_i$ are the positions of the ions and the superscript (i) indicates that the $A_\ell^{(i)}$, $P_{\ell m}^{(i)}$, and $R_\ell^{(i)}$ depend on the chemical species of atom i. The range of the nonlocal pseudopotential extends only up to a sphere of radius $r_c^{(i)}$ around each atomic position $\mathbf{R}_i$. Normally the core radii $r_c^{(i)}$ are chosen so that there is no overlap between the different core spheres. Therefore, the pseudopotentials centered on different atoms commute.

Several factorizations have been derived for the case of three noncommuting operators;[33] a simple method to obtain such factorizations is to use the various two-operator factorizations[24,25] recursively. There are many different ways to do this; we have chosen the factorization that contains the smallest number of nonlocal operators, which is the the computationally most efficient one:

$$e^{-\epsilon\hat{H}} = e^{-(1/6)\epsilon\hat{V}_{\rm nl}} e^{-(1/2)\epsilon\hat{H}_{\rm loc}} e^{-(2/3)\epsilon\hat{D}_{\rm nl}} e^{-1/2\,\epsilon\hat{H}_{\rm loc}} e^{-(1/6)\epsilon\hat{V}_{\rm nl}} + \mathcal{O}(\epsilon^5). \tag{2.37}$$

The operator $e^{-(1/2)\epsilon\hat{H}_{\rm loc}}$ is factorized using Eq. (2.5), and the nonlocal double commutator is

$$\hat{D}_{nl} = \hat{V}_{nl} + \frac{\epsilon^2}{48}[\hat{V}_{nl},[\hat{H}_{\rm loc},\hat{V}_{nl}]]. \tag{2.38}$$

To use the factorization [Eqs. (2.37) and (2.38)] in practical calculations, one needs to evaluate the action of the individual factors on the states $\psi_j(\mathbf{r})$. The only new aspect is the treatment of the nonlocal potential and the nonlocal commutator:

(i) The nonlocal potential, $e^{-\epsilon\hat{V}_{nl}}\psi_j(\mathbf{r})$: as long as the projector functions $P_{\ell m}$ in Eq. (2.36) do not overlap, the exponential series can be summed up.[3]

(ii) The nonlocal double commutator, $e^{-\epsilon\hat{D}_{nl}}\psi_j(\mathbf{r})$: In Ref. 3, we have shown that the exponential series can be evaluated easily when

$$\langle P_{\ell m}^{(i)}|H_{\rm loc}|P_{rs}^{(j)}\rangle = \delta_{ij}\delta_{lr}\delta_{ms}. \tag{2.39}$$

(iii) This assumption is only rigorously satisfied if the local potential is spherically symmetric in the region where the nonlocal projectors $P_{\ell m}$ are different from zero, otherwise the local potential will mix different angular-momentum channels. In the magnetic field case, also the canonical momentum operator mixes different angular momenta. However, such a mixing only affects the convergence rate of the algorithm, but not the final result. We have demonstrated[3] that for realistic pseudopotentials the violation of Eq. (2.39) only deteriorates the convergence rate at unnecessary small time steps.

E. Gauge properties of nonlocal pseudopotentials

For a theory to be gauge invariant, all operators in the Hamiltonian must transform according to Eq. (2.21). Then, all matrix elements of the Hamiltonian are by definition invariant under gauge transforms,

$$\begin{aligned} \langle\psi'|\hat{H}'|\phi'\rangle &= \langle\psi e^{+i(e/\hbar)\chi(\mathbf{r})}|e^{-i(e/\hbar)\chi(\mathbf{r})}\hat{H}e^{+i(e/\hbar)\chi(\mathbf{r})}|e^{-i(e/\hbar)\chi(\mathbf{r})}\phi\rangle \\ &= \langle\psi|\hat{H}|\phi\rangle, \end{aligned} \tag{2.40}$$

and the physics described by $\hat{H}$ is indeed independent of the gauge. Equation (2.21) holds for the canonical momentum operator, and it is trivially fulfilled for local potentials. On the other hand, the transformation properties of pseudopotentials of the type [Eq. (2.36)] are not obvious.

The pseudopotential approximation makes use of the fact that the core electrons are tightly bound to the nucleus and relatively inert to changes in the chemical environment around the atom. They can therefore be assumed to be "frozen," and need to be calculated only once for each chemical species by an all-electron calculation of the free atom. In the pseudopotential approximation, the effect of core electrons is then simulated by an effective nonlocal potential that reproduces the correct all-electron wave functions of the valence states outside a given core radius.

In the presence of an external magnetic field, the all-electron problem would have to be solved using exactly the same vector potential that is used in the pseudopotential calculation. Moreover, since the vector potential $\mathbf{A}(\mathbf{r})$ breaks translational invariance, the core wave functions depend on

the position of the atom. Under a gauge transformation $\mathbf{A}(\mathbf{r}) \rightarrow \mathbf{A}'(\mathrm{r}) = \mathbf{A}(\mathbf{r}) + \chi(\mathbf{r})$, the core wave functions, and in turn also the projector functions $|P_{\ell m}^{(i)}\rangle$, should transform as

$$\langle \mathbf{r} - \mathbf{R}_i \, | P_{\ell m}^{\mathbf{A},(i)} \rangle \rightarrow \langle \mathbf{r} - \mathbf{R}_i \, | P_{\ell m}^{\mathbf{A}',(i)} \rangle = e^{-i(e/\hbar)\chi(r)} \langle \mathbf{r} - \mathbf{R}_i | P_{\ell m}^{\mathbf{A},(i)} \rangle. \tag{2.41}$$

Consequently, the nonlocal potential operator [Eq. (2.36)] is a gauge-invariant operator transforming according to Eq. (2.21).

Having to generate separate pseudopotentials for each field strength and atom position is, of course, rather impractical. The problem of finding versatile nonlocal potentials in a magnetic field has been examined by Pickard and Mauri[22,34] using the projector-augmented wave (PAW) formalism, and by Ismail–Beigi *et al.*[35] in a Feynman path-integral approach. Pickard and Mauri found that for an atom located at the gauge origin, the effect of a magnetic field on the projector functions is negligible for norm-conserving pseudopotentials. Thus, one can use the potentials generated by standard pseudopotential packages for $\mathbf{B}=0$ also for calculations in an external magnetic field. For atoms not located at the gauge origin, one has to take into account the phase factor (2.41) that the projectors pick up under translations.

The bottom line conclusion, drawn from Eq. (2.41), is that gauge invariance[22] of nonlocal Hamiltonians is maintained by *postulating* that the projectors transform according to Eq. (2.21), and hence, the nonlocal part of the potential transforms under gauge transformation such as

$$\begin{aligned} \hat{V}_{nl}(\mathbf{r},\mathbf{r}') \rightarrow \hat{V}'_{nl}(\mathbf{r},\mathbf{r}') &= e^{-i\frac{e}{\hbar}\chi(\mathbf{r})} \hat{V}_{nl}(\mathbf{r},\mathbf{r}') e^{i\frac{e}{\hbar}\chi(\mathbf{r})} \\ &= e^{-i\frac{e}{\hbar}\chi(\mathbf{r})} \sum_i v_{nl}^{(i)}(\mathbf{r}-\mathbf{R}_i, \mathbf{r}'-\mathbf{R}_i) e^{i\frac{e}{\hbar}\chi(\mathbf{r})}. \end{aligned} \tag{2.42}$$

For numerical applications, the practically only interesting gauge transformation is, in Landau gauge, a translation of the origin, i.e.,

$$\mathbf{A}(\mathbf{r}) = -By\mathbf{e}_x \rightarrow \mathbf{A}'(\mathbf{r}) = -B(y-y_0)\mathbf{e}_x, \quad \chi(\mathbf{r}) = By_0 x, \tag{2.43}$$

so that the projectors are moved to their destination $\mathbf{R}_i = (x_i, y_i, z_i)$ by the transformation

$$\langle \mathbf{r} - \mathbf{R}_i | P_{\ell m}^{(i)} \rangle = e^{-i\frac{e}{\hbar}By_i x} \langle \mathbf{r} | P_{\ell m}^{(i)} \rangle. \tag{2.44}$$

In that case, the gauge function is relatively slowly varying over atomic distances whereas the $P_{\ell m}^{(i)}(r)$ are, in the vicinity of the ion cores, rapidly varying functions of position.

III. MAGNETIC SUSCEPTIBILITY AND NMR SHIFTS

The current density corresponding to the self-consistent Kohn–Sham orbitals $\psi_j(\mathbf{r})$ is

$$\mathbf{j}(\mathbf{r}) = \frac{e}{2m} \sum_j [\psi_j^* \Pi \psi_j + \psi_j (\Pi \psi_j)^*] = \frac{e}{m} \sum_j \Re e\{\psi_j^* \Pi \psi_j\}, \tag{3.1}$$

where the sum goes over all occupied states. To be rigorously gauge invariant, the action of the canonical momentum operator is calculated according to Eq. (2.17) applied to the states ψ_j. In homogeneous magnetic fields, this can again be done very efficiently in Fourier space, *cf*. Equation (2.32).

The magnetic-susceptibility tensor χ_{ij} is defined as the weak-field limit of the ratio between the magnetic field $\mathbf{H}$ and the magnetization $\mathbf{M} = \frac{1}{\mu_0}\mathbf{B} - \mathbf{H}$,

$$\chi_{ij} = \frac{\partial M_i}{\partial H_j} = \frac{\partial B_j}{\partial H_j} \frac{\partial M_i}{\partial B_j}. \tag{3.2}$$

The magnetic susceptibilities are usually very small compared to unity

$$\frac{\partial B_j}{\partial H_j} = \mu_0 \left(1 + \frac{\partial M_j}{\partial B_j} \right) = \mu_0 (1 + \chi_{jj}) \approx \mu_0, \tag{3.3}$$

where μ_0 is the vacuum permeability. We can therefore calculate the susceptibility tensor as

$$\chi_{ij} = \mu_0 \frac{\partial M_i}{\partial B_j}. \tag{3.4}$$

The magnetic-dipole moment generated by the current density [Eq. (3.1)] is

$$\mathbf{m} = \frac{1}{2} \int \mathbf{r} \times \mathbf{j}(\mathbf{r}) d^3\mathbf{r}. \tag{3.5}$$

Assuming a density of $n = N/V$ molecules per unit volume, the dimensionless bulk susceptibility is

$$\chi_{ij} = \frac{N\mu_0}{V} \frac{\partial}{\partial B_j} m_i. \tag{3.6}$$

Experimental values for the susceptibility are usually given as molar susceptibilities χ^m in units of $\mathrm{cm}^2\ \mathrm{mol}^{-1}$,

$$\chi_{ij}^m = N_A \mu_0 \frac{\partial m_i}{\partial B_j}. \tag{3.7}$$

The chemical shift tensor is defined as the ratio between the induced magnetic field and the external field,

$$\sigma_{ij}(\mathbf{R}) = \frac{\partial B_i^{\mathrm{ind}}(\mathbf{R})}{\partial B_j^{\mathrm{ext}}}. \tag{3.8}$$

The induced field is determined by the current density [Eq. (3.1)] through the Biot–Savart law,

$$\mathbf{B}^{\mathrm{ind}}(\mathbf{r}) = \frac{\mu_0}{4\pi} \int d^3r' \frac{\mathbf{r}' - \mathbf{r}}{|\mathbf{r}' - \mathbf{r}|^3} \times \mathbf{j}(\mathbf{r}'). \tag{3.9}$$

Due to the singularity at $\mathbf{r}' = \mathbf{r}$, it is difficult to evaluate the integral in coordinate space. However, Eq. (3.9) can be easily calculated in reciprocal space,[19]

$$\mathbf{B}^{\mathrm{ind}}(\mathbf{G}\neq 0) = -\mu_0 i \frac{\mathbf{G}}{|\mathbf{G}|^2}\times \mathbf{j}(\mathbf{G}). \tag{3.10}$$

The $\mathbf{G}=0$ component of the induced field depends on the bulk magnetic susceptibility,

$$\mathbf{B}^{\mathrm{ind}}(\mathbf{G}=0) = \kappa\chi\mathbf{B}^{\mathrm{ext}}, \tag{3.11}$$

and a prefactor κ depending on the shape of the sample.[19]

Experiments often only measure the isotropic susceptibilities and NMR shifts $\bar{\chi}$ and $\bar{\sigma}$,

$$\bar{\chi} = \frac{1}{3}\mathrm{tr}\chi_{ij}, \quad \bar{\sigma}(\mathbf{R}) = \frac{1}{3}\mathrm{tr}\sigma_{ij}(\mathbf{R}). \tag{3.12}$$

Experimental values of the dimensionless shift are usually given in ppm, i.e., in units of 10^{-6}.

IV. CONVERGENCE AND STABILITY TESTS

The numerical calculations to be discussed in this section have been performed for a homogeneous magnetic field in the z direction. We have used Landau gauge,

$$\mathbf{A}(\mathbf{r}) = B(x-x_0)\mathbf{e}_y,$$

where x_0 is the position of the gauge origin. The functions $f_j(\mathbf{r})$ defined in Eq. (2.16) thus read

$$f_y(\mathbf{r}) = B(x-x_0)y, \quad f_x(\mathbf{r}) = f_z(\mathbf{r}) = 0. \tag{4.1}$$

To show the effect of a gauge-invariant discretization of the problem, we have compared results for two different discretizations of the canonical momentum operator:

(1) gauge-invariant discretization:

$$\Pi^2 = -\hbar^2\left[\left[\frac{\partial^2}{\partial x^2}\right]_n + e^{-i(e/\hbar)B(x-x_0)y}\left[\frac{\partial^2}{\partial y^2}\right]_n e^{+i(e/\hbar)B(x-x_0)y} + \left[\frac{\partial^2}{\partial z^2}\right]_n\right] \tag{4.2}$$

(2) Lagrange discretization:

$$\Pi^2 = -\hbar^2\left[\frac{\partial^2}{\partial x^2}+\frac{\partial^2}{\partial y^2}+\frac{\partial^2}{\partial z^2}\right]_n - 2ie\hbar B(x-x_0)\left[\frac{\partial}{\partial y}\right]_n + e^2B^2(x-x_0)^2, \tag{4.3}$$

In both cases, the derivatives have been approximated by the finite-difference representations (2.23) and (2.24) of order $n=9$.

A. The Fock–Darwin Model

We address the discretization problem first. This is best done by solving a problem whose exact solution is known. That way, we can demonstrate the accuracy, the convergence rate, and stability of our algorithm without having to deal with pseudopotentials that have their intrinsic convergence issues discussed above. For that purpose, we have studied the three-dimensional version of the well-known Fock–Darwin model,[36,37] i.e., an electron in a uniform magnetic field and a harmonic potential. The Hamiltonian of this model is

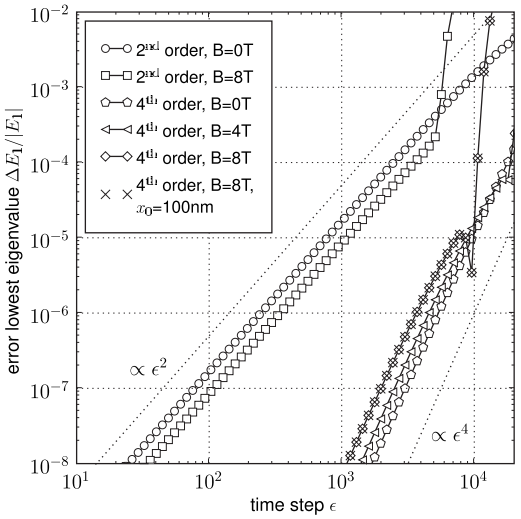

FIG. 1. The figure shows the relative error of the lowest eigenvalue of noninteracting electrons in a parabolic potential in dependence of the imaginary time step ϵ. Results for the second and fourth order algorithms are shown for three different magnetic fields ($B=0,4,8$ T). For $B=8$ T, crosses indicate the results obtained when the gauge origin is not at the potential minimum, but shifted by $x_0=100$ nm in x direction. These data points lie on top of the data with no shift of the gauge origin (diamonds), as a result of gauge invariance of the theory. Dotted lines show the functions ϵ^2 and ϵ^4 as guides to verify the power-law convergence.

$$\hat{H} = \frac{1}{2m^*}[-i\hbar\nabla + e\mathbf{A}_{\mathrm{ext}}(\mathbf{r})]^2 + \frac{m^*}{2}\omega_0^2 r^2, \tag{4.4}$$

where m^* is the effective mass of the electron. We allow for such an effective mass to describe a three-dimensional quantum dot in an external matrix. The eigenvalues of the Schrödinger equation can be calculated analytically,

$$E_{nm\ell} = \hbar\omega_+\left(n+\frac{1}{2}\right) + \hbar\omega_-\left(m+\frac{1}{2}\right) + \hbar\omega_0\left(\ell+\frac{1}{2}\right), \tag{4.5}$$

with

$$\omega_\pm = \Omega \pm \frac{\omega_c}{2}, \quad \Omega = \sqrt{\omega_0^2+\frac{\omega_c^2}{4}} \tag{4.6}$$

and the cyclotron frequency $\omega_c = \frac{eB}{m^*}$.

Although the evolution operator [Eq. (2.3)] for this problem can be calculated exactly, we have used the factorizations (2.4) and (2.5) for the purpose of demonstrating the convergence of our method and in particular to show the comparison between the second and fourth order algorithms.

In our calculations, we have used GaAs material parameters (effective mass $m^*=0.066m_e$, dielectric constant $\epsilon=12.7$); the harmonic potential has been chosen such that the level spacing at zero field is 1.57 meV. The spatial extent of the resulting system is roughly 200 nm. The numerical calculations have been performed on a grid of 96^3 points with a mesh spacing of $h=3.6$ nm.

Figure 1 shows the convergence of the lowest eigenvalue

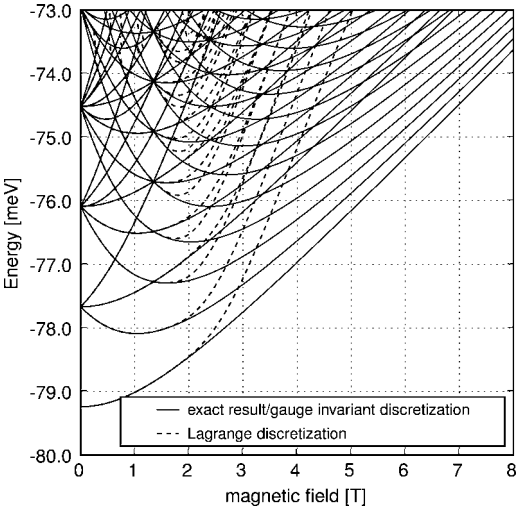

FIG. 2. Energy eigenvalues of a three-dimensional parabolic quantum dot in an external magnetic field, using an effective-mass approximation with GaAs parameters ($m^*=0.066m_e$). The solid lines show the analytic results that are indistinguishable from the results of the gauge-invariant discretization, the dashed lines denote eigenvalues calculated using the Lagrange discretization. The numerical calculations were performed on a grid of 96^3 points with the gauge origin shifted 100 nm away from the center of the dot (the size of the dot is roughly 200 nm). One can see that Lagrange discretization fails to reproduce the Fock–Darwin spectrum for field strengths larger than 2 T.

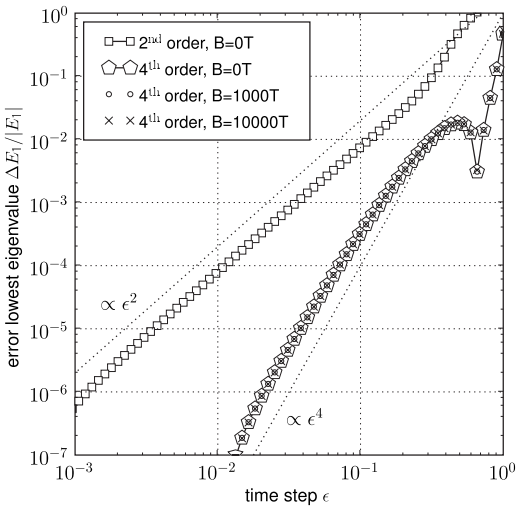

FIG. 3. The figure shows the relative error of the lowest eigenvalue of electrons in a C_6H_6 molecule in dependence of the imaginary time step ϵ. Results for the second and fourth order algorithm are shown for three different magnetic fields ($B=0$, 1000, 1000 T). The data points for the fourth order algorithm lie on top of each other, indicating that even fields of up to 10000 Tesla do not deteroriate fourth order convergence. The functions ϵ^2 and ϵ^4 are shown as guides to verify the power-law convergence.

of noninteracting electrons in the parabolic potential defined above as a function of the imaginary time step ϵ. Technically the calculation is carried out by starting at a large time step with a simple set of initial wave functions. These are iterated to convergence in the sense that the eigenvalue/function pair changes by less than $\delta=10^{-8}$ for given ϵ. Then the time step is reduced, and the process is repeated.

The figure shows that we have perfect fourth order convergence practically independently of the magnetic-field strength. We also see no visible change of the convergence rate as a function of the gauge origin. To assess the relative performance of the two algorithms, one must know that it takes, for fixed value of ϵ, about the same total imaginary propagation time $N\epsilon$, where N is the number of iterations, for each algorithm to obtain a given desired accuracy δ. Thus, the main advantage of the fourth order method is that one reaches a high accuracy at larger values of ϵ. One can read off the performance difference directly from Fig. 1: For example, to obtain an accuracy of 10^{-6}, one needs a time step $\epsilon\approx 300$ in the second order algorithm, whereas the same accuracy is reached with $\epsilon\approx 4000$ in the fourth order method. In other words, the second order algorithm needs about ten times more iterations. Given that one iteration in the fourth order method takes roughly twice as long as one iteration in the second order method, the speed advantage is about a factor of five. Requiring a higher accuracy of 10^{-8}, which is often needed to anneal the ionic configuration to its ground state, quickly improves the speed advantage of the fourth order method to a factor of about 50.

Figure 2 compares the Fock–Darwin spectra obtained using the Lagrange [Eq. (4.3)] and gauge-invariant [Eq. (4.2)] discretization schemes with the exact formula (4.5). For the Fock–Darwin model, the "natural" choice of the gauge origin is of course the minimum of the parabolic potential. In more realistic systems, however, there is no such unique choice; consider, e.g., an array of quantum dots. To mimic the problems posed by realistic calculations, while still being able to compare the numerical results to the exact formula, we have performed the calculation of the Fock–Darwin spectra with a gauge origin shifted by about 100 nm away from the center of the dot. The figure shows that the results obtained using the gauge-invariant discretization are indistiguishable from the exact data. On the other hand, Lagrange discretization yields energy levels that deviate markedly from the exact ones at fields above 2 T.

B. Convergence for a realistic system

Let us now turn to the analysis of the convergence for a realistic system. As pointed out above, the deviation of the local density around the ion cores, as well as the terms $e^{-i(e/\hbar)f_j(\mathbf{r})}$, from spherical symmetry can destroy the exact fourth order convergence of the algorithm. Figure 3 shows the convergence as a function of time step for a C_6H_6 molecule for three magnetic-field strengths; to separate the two effects, we have carried out our calculations up to unrealistically high magnetic fields. As in earlier work,[3] tests of the convergence of the second and fourth order eigensolvers have been performed as follows: We have first self-consistently solved the Kohn–Sham equations, taking the Perdew–Wang density functional[38] and employing Troullier–Martins[39] pseudopotentials generated by the program FHI98PP.[40] We have then taken the electron density and the corresponding Kohn–Sham potential as a fixed local field

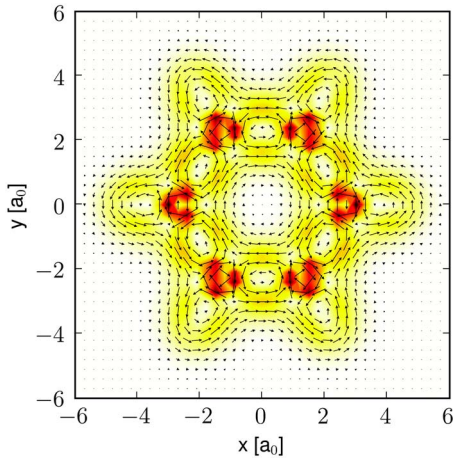

FIG. 4. (Color online) Current density of a C_6H_6 molecule in the symmetry plane, in an external magnetic field of 1 T perpendicular to this plane. The field is pointing into the plane of the figure. The gauge-invariant discretization scheme [Eq. (4.2)] has been used to perform several calculations in Landau gauge with different gauge origins between $x_0=0.0a_0$ (center of the molecule) and $x_0=50.0a_0$, all showing the same result.

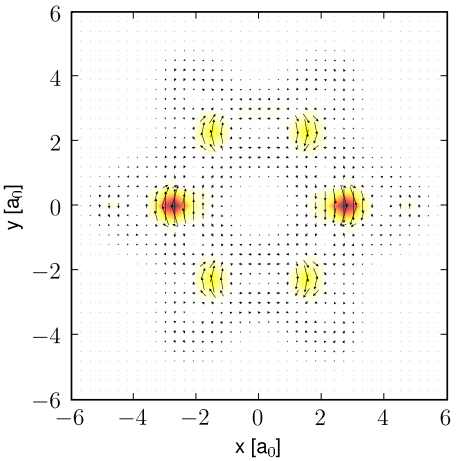

FIG. 5. (Color online) Current density of a C_6H_6 molecule in the symmetry plane, in an external magnetic field of 1 T perpendicular to this plane. The field is pointing into the plane of the figure. The calculation has been performed using the Lagrange discretization scheme [Eq. (4.3)] and Landau gauge, with the gauge origin positioned at $x_0=0.0a_0$, the center of the molecule.

and have solved again the eigenvalue problem, using as initial guess for the evolution the wave functions of a particle in a box. The process was then repeated, as described in the previous section, for a sequence of time steps ϵ.

Figure 3 shows, at time steps $\epsilon < 10^{-6}$, slight indications of the expected effect that the fourth order power law is violated when the local Kohn–Sham potential is not spherically symmetric in the vicinity of the ion cores. This is due to our approximate treatment of the double commutator as discussed above. On the other hand, we see practically no effect of the magnetic field even up to unreasonably high-field strengths. Independent of that we see again the improvement of convergence by the fourth order algorithm, which is comparable to the case of the Fock–Darwin model.

Figure 4 shows the current density in the symmetry plane of a C_6H_6 molecule in an external field of 1 T perpendicular to the plane (pointing inward). The gauge-invariant discretization has been used to calculate the current density, we have verified that different gauge origins between $x_0=0.0a_0$ (center of the molecule) and $x_0=50a_0$ all yield the same result. One can see the paramagnetic ring current on the inside of the ring, and a diamagnetic current flowing around the outside of the molecule. There are additional current loops alongside the C–C bonds, and around the individual ions. From the direction of these currents, one would conclude a deshielding (i.e., a diamagnetic shift) of the hydrogen atoms, and a positive shift of the carbon atoms. Figure 5 shows the same data as Fig. 4, but was calculated using Lagrange discretization with the gauge origin positioned at the center of the molecule. One can see that the structure of the current density is strongly distorted compared to Fig. 4, due to the violation of gauge invariance caused by the Lagrange discretization.

Figure 6 shows the hydrogen NMR shifts calculated from the current densities depicted in Figs. 4 and 5 as a function of the gauge origin. Gauge-invariant discretization yields the same values for all (chemically equivalent) hydrogen atoms, while in Lagrange discretization the shift strongly depends on the distance of the atom to the gauge origin.

V. MAGNETIC SUSCEPTIBILITIES AND NMR SHIFTS OF VARIOUS MOLECULES

We have implemented the gauge-invariant discretization of the canonical momentum operator in the package limerec,[41] a real-space DFT code using the fourth order diffusion method to solve the Kohn–Sham equations. We have used Troullier–Martins[39] pseudopotentials generated by the program FHI98PP,[40] and the Perdew–Wang LDA density

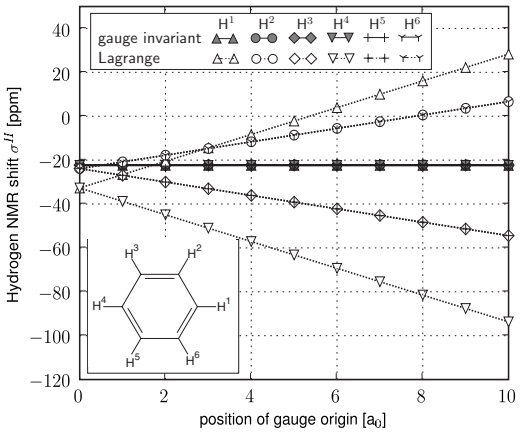

FIG. 6. Hydrogen NMR shifts σ^H for a C_6H_6 molecule, calculated using the Lagrange [Eq. (4.3)] and gauge-invariant [Eq. (4.2)] discretization schemes. The numbering of the hydrogen atoms is shown in the inset. The gauge-invariant calculation (solid lines) yields the same NMR shifts for all (chemically equivalent) hydrogen atoms, irrespective of their position relative to the gauge origin. The results obtained using Lagrange discretization (dotted lines) strongly depend on the location of the gauge origin.

TABLE I. Experimental and calculated values of the isotropic susceptibility for a set of small molecules. Also see Fig. 7.

	Susceptibility $\bar{\chi}[10^{-6}$ cm^3 mol$^{-1}]$						
Molecule	Exp.	This work	CSGT[c]	CSGT[d]	CONV[e]	IGAIM[f]	CSGT[g]
H_2	−4.0 [a]	−4.2	—	—	—	—	—
H_2O	−13.1 [a]	−14.5	−13.3	−14.0	—	—	—
CH_4	−17.4 [b]	−19.7	−18.2	−18.6	−18.9	−18.7	−18.7
C_2H_6	−26.8 [b]	−29.1	−29.4	−27.6	−29.9	−29.0	−28.7
C_2H_4	−18.8 [b]	−20.0	−22.9	−20.6	−21.5	−21.0	−20.9
C_2H_2	−20.8 [b]	−22.5	−24.6	−23.3	−23.1	−22.7	−22.7
C_6H_6	−54.8 [b]	−54.9	−67.4	−57.4	−87.7	−59.7	−57.5
TMS	−74.8 [a]	−75.8	—	—	—	—	—

[a]Experimental values taken from Ref. 44.
[b]Experimental values taken from Ref. 18.
[c]Sebastiani,[19] $\Delta j=0$.
[d]Sebasitani,[19] full calculation.
[e]Keith and Bader[18] CONV (single gauge origin at charge centroid).
[f]Keith and Bader[18] IGAIM.
[g]Keith and Bader[18] CSGT.

functional.[38] All calculations were performed on a real-space grid with a mesh size of $0.3a_0$, the molecular geometries have been annealed before calculating the magnetic properties.

We have solved the Kohn–Sham equations for a fixed magnetic field $\mathbf{B}^{\text{ext}}$, and have then calculated the current density $\mathbf{j}(\mathbf{r};\mathbf{B}^{\text{ext}})$ through Eq. (3.1). From the current density, the dipole moment $\mathbf{m}(\mathbf{B}^{\text{ext}})$ and the induced field $\mathbf{B}^{\text{ind}}(\mathbf{r};\mathbf{B}^{\text{ext}})$ were calculated using Eqs. (3.5) and (3.10). We have verified that $\mathbf{m}(\mathbf{B}^{\text{ext}})$ and $\mathbf{B}^{\text{ind}}(\mathbf{r};\mathbf{B}^{\text{ext}})$ are perfectly linear up to magnetic fields of a few thousand Tesla. Since for closed-shell systems $\mathbf{j}(\mathbf{r})=0$ for $\mathbf{B}^{\text{ext}}=0$, we have generally used a single self-consistent calculation at a field of 1 Tesla to determine the derivatives (3.7) and (3.8). The relative error of this approximation compared to using linear regression with 20 self-consistent calculations for different fields is about 10^{-5}. Consequently, the calculation of χ_{ij} and σ_{ij} requires the self-consistent calculation of the complex Kohn–Sham orbitals for three orthogonal directions of the external field. The computational effort is thus the same as for a perturbative calculation, which would require six calculations using real wave functions.

When pseudopotentials are used, the core wave functions are not taken into account at all, and the valence wave functions have an incorrect shape inside the core region. This approximation describes those properties quite well that are dominated by regions outside the core, e.g., chemical bonding or total energies. Nuclear shielding, on the other hand, is sensitive to the structure of the all-electron wave functions in the core region, since the interaction between the nuclear spin and the electronic current is proportional to r^{-2}. However, it has been shown[22,42] that the error caused by the

TABLE II. Experimental and calculated values of the Hydrogen NMR shift for a set of small molecules. Also see Fig. 8.

	Hydrogen shift $\bar{\sigma}^H$ [ppm]				
Molecule	Exp.	This work	CSGT[c]	CSGT[d]	MPL[e]
H_2	−26.2 [a]	−26.1	—	—	−25.9
H_2O	−30.1 [f]	−30.8	−29.3	−29.3	—
CH_4	−30.6 [a]	−30.9	−30.9	−30.7	−30.7
C_2H_6	−23.7 [a]	−30.0	−30.4	−29.9	−29.7
C_2H_4	−25.4 [a]	−24.7	−26.3	−25.4	−24.5
C_2H_2	−29.3 [a]	−28.6	−29.6	−29.4	−28.6
C_6H_6	−29.9 [b]	−22.9	−25.5	−24.0	—

[a]Experimental values taken from Ref. 20.
[b]Experimental values taken from Ref. 19.
[c]Sebastiani,[19] $\Delta j=0$.
[d]Sebastiani,[19] full calculation.
[e]Mauri[20]
[f]Experimental values taken from Ref. 45.

TABLE III. Experimental and calculated values of the ^{13}C NMR shift for a set of small molecules. Also see Fig. 9.

	Carbon shift $\bar{\sigma}^C$ [ppm]						
Molecule	Exp.	This work	CSGT[b]	CSGT[c]	CONV[d]	IGAIM[e]	CSDGT[f]
CH_4	195.1[a]	193.7	173.0	178.0	196.0	195.5	195.3
C_2H_6	180.9[a]	178.9	184.4	160.0	184.4	183.4	183.2
C_2H_4	64.5[a]	83.3	64.1	62.0	64.1	63.4	63.1
C_2H_2	117.3[a]	129.9	120.4	125.0	120.4	118.1	118.1
C_6H_6	57.9[a]	84.5	71.9	67.0	71.9	61.5	60.2

[a]Experimental values taken from Ref. 18.
[b]Sebastiani,[19] $\Delta j=0$.
[c]Sebastiani,[19] full calculation.
[d]Keith and Bader[18] CONV (single gauge origin at charge centroid).
[e]Keith and Bader[18] IGAIM.
[f]Keith and Bader[18] CSDGT (continous set of damped gauge transforms): CSGT with an additional, empirically determined damping factor.

pseudopotential approximation is in many cases almost constant with respect to changes in the chemical environment of the atom. This constant correction is in practice obtained by the same convention that is also used in experiments: the valence electron shieldings are calculated relative to a reference molecule with a known absolute shielding. A commonly used reference is tetramethylsilane [TMS, $Si(CH_3)_4$], with an absolute carbon shielding of $\sigma^C_{\mathrm{TMS}}=188.1$ ppm.[43]

We compare our results to experimental values and to different numerical calculations (see Tables I–III). Sebastiani[19] has used DFT with the Becke, Lee, Young, and Parr (BLYP) gradient corrected functional, Goedecker pseudopotentials, and the CSGT method. He provides two different sets of results: "full calculation," which is only suitable for isolated systems, and "$\Delta j=0$," which also works for periodic systems. Keith[18] has performed all-electron calculations using the "coupled perturbed Hartree–Fock" (CPHF) method, and compares the CONV, IGAIM and CSGT methods to deal with the gauge origin problem. He obtained carbon shifts using an additional empirical "damping factor," a method termed CSDGT (continuous set of damped gauge transforms). Mauri *et al.*[20] have used DFT, the local-density approximation, Troullier–Martins pseudopotentials, and the MPL method.

Figure 7 shows the magnetic susceptibilities obtained by the different methods and the corresponding experimental values. Overall, the agreement of our calculations with both experimental values and other calculations is very good. Benzene seems to be a notable case, the deviation between various methods is much larger for this molecule. Especially, the CONV method (single gauge origin) yields a result that is about 60 percent off the experimental value. Also, Sebastiani's $\Delta j=0$ calculation differs remarkably from experiment. We suspect that this is due to the delocalized electron system in the benzene ring, where the gauge origin problem plays a more important role than in the smaller molecules, where electrons are more localized.

Figure 8 compares the hydrogen NMR shifts σ^H for the different methods. Again, the agreement with experiment is quite satisfactory, but one can see that for the molecules containing only single bonds (H_2, CH_4, and C_2H_6) the shifts are predicted much more accurately than for molecules containing double and triple bonds (C_2H_4, C_2H_2, and C_6H_6). Since the LDA results of Mauri are quite close to our results, while Sebastiani's calculations using the BLYP gradient corrected functional are closer to experiment, this could indicate that LDA describes these types of bonds less accurately, as already supposed by Mauri.[20]

The agreement of the calculated carbon shifts, shown in Fig. 9, with experiment is less satisfactory for most methods. Here, the limitations of the pseudopotential approximation become apparent: the rigid additive correction for the pseudopotential was calculated using TMS (tetramethylsilane) as a reference. For similar chemical environments

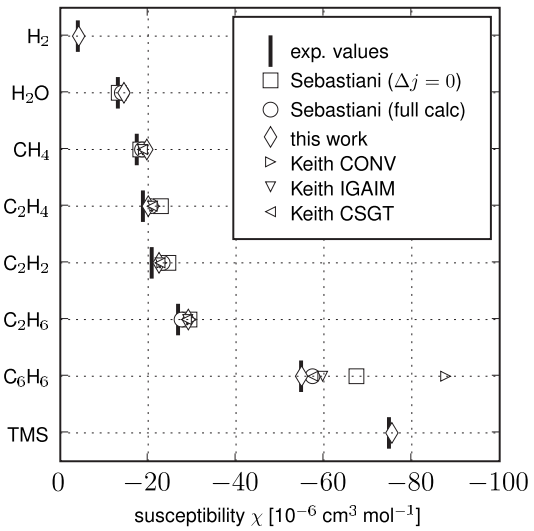

FIG. 7. Calculated magnetic susceptibilities and experimental values for a sample of small molecules. See Table I for the numerical values. Squares and circles depict values calculated by Sebastiani (Ref. 19) using CSGT, triangles depict results obtained by Keith (Ref. 18) in an all-electron CPHF calculation using the CONV, IGAIM, and CSGT methods, diamonds show the results of this work. TMS is the molecule tetramethylsilane.

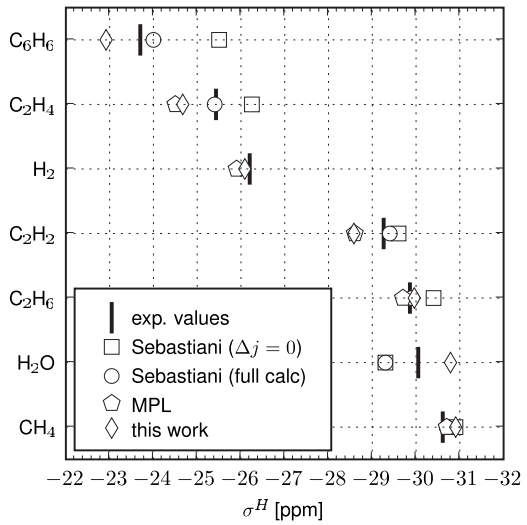

FIG. 8. Calculated and experimental values of hydrogen NMR shifts for a set of small molecules. Squares and circles denote values calculated by Sebastiani (Ref. 19) using CSGT, pentagons denote simulations by Mauri using the MPL method, and diamonds show the results of this work. See Table II for the numerical values.

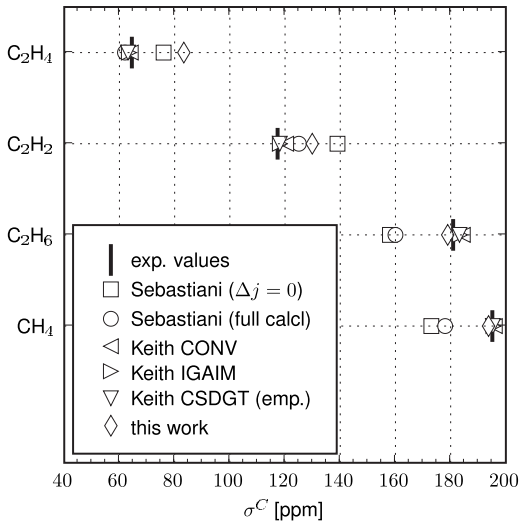

FIG. 9. Calculated and experimental values of carbon NMR shifts for a set of small molecules. Squares and circles denote values calculated by Sebastiani (Ref. 19) using CSGT, triangles denote results obtained by Keith (Ref. 18) in an all-electron CPHF calculation using the CONV, IGAIM, and CSGT methods, diamonds show the results of this work. See Table III for the numerical values.

(CH_4 and C_2H_6), the carbon shifts are predicted very well. But the rigid correction fails to describe the change in coordination when going to different hybridization states of the carbon atom, an effect that adds up to the error due to LDA described above. Consequently, the all-electron calculations of Keith yield much more accurate predictions for the carbon shifts than the pseudopotential-based methods.

VI. CONCLUSIONS

We have presented in this article a full implementation of DFT in an arbitrarily strong, homogeneous magnetic field, employing a real-space grid to represent Kohn–Sham orbitals, electron density, and potential. The eigenvalue/eigenstate pairs for a fixed potential are determined using a fourth order factorization of the evolution operator in imaginary time. A judicious discretization of the kinetic-energy operator has permitted a formulation that is gauge invariant in any discretization. The correspondence between the harmonic oscillator and the particle in a homogeneous magnetic field permitted an exact calculation of the exponential of the canonical kinetic-energy operator[28] with practically no computational overhead.

We have used here the generalization of the diffusion method to nonlocal pseudopotentials[3] of the Kleinman–Bylander type, which allow for quantitative simulations of most *s*, *p*, and *d* electron elements and complexes within the LDA. The high order of the factorization allows the method to efficiently compute the eigenpairs, with a computational cost that is typically one order of magnitude less than that required when employing the second-order factorization. The rigorous fourth order convergence is slightly compromised by numerical sacrifices that were made in the treatment of the nonlocal components of the potential, but this deviation from fourth order has no *practical* consequences, i.e., it alters neither the result, nor the speed of convergence. We have also demonstrated that a magnetic field does not visibly deteriorate the convergence rate.

Our results are consistent with earlier DFT calculations cited above. Remaining differences with experiments should be attributed to the local density and the pseudopotential approximation but are free from any issues concerned with the choice of the gauge origin. We should again point out the simplicity of the method: the core of the algorithm, namely the propagation of the states, is a matter of a few lines of code,[27] the most complicated part of the method is the propagation with nonlocal pseudopotentials. In the present problem, the real-space formulation has the further significant advantage that the problem can be formulated in a manifestly gauge-invariant way. This advantage is immediately lost when the wave functions are represented in a basis other than a real-space grid or a plane-wave basis. Then, the products $e^{i(e/\hbar)f_j(\mathbf{r})}\psi(\mathbf{r})$ would have to be expanded again in a basis, which would lead to additional discretization errors.

ACKNOWLEDGMENTS

This work was supported the Austrian Science Fund FWF under Grant No. P18134 as well as the Austrian Academic Exchange Services ÖAD (No. 11/2006) and the Spanish MEC (No. HU2005-0033) through a bilateral collaborative project. We also would like to thank S. A. Chin and E. Hérnandez for useful discussions and correspondence.

[1] J. Auer, E. Krotscheck, and S. A. Chin, J. Chem. Phys. **115**, 6841 (2001).
[2] M. Aichinger and E. Krotscheck, Comput. Mater. Sci. **34**, 188 (2005).
[3] E. R. Hernández, S. Janecek, M. S. Kaczmarski, and E. Krotscheck, Phys. Rev. B **75**, 075108 (2007).
[4] W. Kohn and L. J. Sham, Phys. Rev. **140**, A1133 (1965).
[5] W. Kohn and P. Vashishta, in *Theory of the Inhomogeneous Electron Gas*, edited by S. Lundqvist and N. H. March (Plenum, New York, 1983), p. 79.
[6] M. Aichinger, S. A. Chin, and E. Krotscheck, Comput. Phys. Commun. **171**, 197 (2005).
[7] M. Aichinger, S. A. Chin, E. Krotscheck, and E. Räsänen, Phys. Rev. B **73**, 195310 (2006).
[8] J. Wosnitza, J. Hagel, N. Kozlova, D. Eckert, K.-H. Müller, C. H. Mielke, G. Goll, T. Yoshino, and T. Takabatake, Physica B (Amsterdam) **346-347**, 127 (2004).
[9] N. Kozlova *et al.*, Phys. Rev. Lett. **95**, 086403 (2005).
[10] J. Wosnitza *et al.*, New J. Phys. **8**, 174 (2006).
[11] Z. Jiang, Y. Zhang, Y.-W. Tan, J. A. Jaszczak, H. L. Stormer, and P. Kim, Int. J. Mod. Phys. B **21**, 1123 (2007).
[12] T. Helgaker, M. Jazuński, and K. Ruud, Chem. Rev. (Washington, D.C.) **99**, 293 (1999).
[13] R. M. Stevens, R. M. Pitzer, and W. N. Lipscomb, J. Chem. Phys. **38**, 550 (1963).
[14] W. N. Lipscomb, Adv. Magn. Reson. **2**, 137 (1966).
[15] M. Schindler and W. Kutzelnigg, J. Chem. Phys. **76**, 1919 (1982).
[16] W. Kutzelnigg, J. Mol. Struct.: THEOCHEM **202**, 11 (1989).
[17] T. A. Keith and R. F. W. Bader, Chem. Phys. Lett. **194**, 1 (1992).
[18] T. A. Keith and R. F. W. Bader, Chem. Phys. Lett. **210**, 223 (1993).
[19] D. Sebastiani and M. Parrinello, J. Phys. Chem. A **2001**, 1951 (2000).
[20] F. Mauri, B. G. Pfrommer, and S. G. Louie, Phys. Rev. Lett. **77**, 5300 (1996).
[21] L. Kleinman and D. M. Bylander, Phys. Rev. Lett. **48**, 1425 (1982).
[22] C. J. Pickard and F. Mauri, Phys. Rev. B **63**, 245101 (2001).
[23] M. Suzuki, in *Computer Simulation Studies in Condensed Matter Physics*, edited by D. P. Landau, K. K. Mon, and H.-B. Schüttler (Springer, Berlin, 1996), Vol. VIII, pp. 1–6.
[24] S. A. Chin, Phys. Lett. A **226**, 344 (1997).
[25] S. A. Chin and C. R. Chen, J. Chem. Phys. **117**, 1409 (2002).
[26] S. Jang, S. Jang, and G. A. Voth, J. Chem. Phys. **115**, 7832 (2001).
[27] S. Janecek and E. Krotscheck, Comput. Phys. Commun. **178**, 835 (2008).
[28] R. P. Feynman, *Statistical Mechanics*, Advanced Books Program (Westview, Boulder, 1998).
[29] C. Cohen-Tannoudji, B. Diu, and F. Laloe, *Quantum Mechanics* (Wiley, New York, 1977).
[30] Z. F. Ezawa, *Quantum Hall Effects—Field Theoretical Approach and Related Topics* (World Scientific, Singapore, 2000).
[31] M. Dvornikov, arXiv:math.NA/0306092v4 (unpublished).
[32] T. L. Beck, Rev. Mod. Phys. **72**, 1041 (2000).
[33] H. A. Forbert and S. A. Chin, Phys. Rev. B **63**, 144518 (2001).
[34] C. J. Pickard and F. Mauri, Phys. Rev. Lett. **91**, 196401 (2003).
[35] S. Ismail-Beigi, E. K. Chang, and S. G. Louie, Phys. Rev. Lett. **87**, 087402 (2001).
[36] V. Fock, Z. Phys. **47**, 446 (1928).
[37] C. G. Darwin, Proc. Cambridge Philos. Soc. **27**, 86 (1930).
[38] J. P. Perdew and Y. Wang, Phys. Rev. B **45**, 13244 (1992).
[39] N. Troullier and J. L. Martins, Phys. Rev. B **43**, 1993 (1991).
[40] M. Fuchs and M. Scheffler, Comput. Phys. Commun. **119**, 67 (1999).
[41] http://www.limerec.net
[42] T. Gregor, F. Mauri, and R. Car, J. Chem. Phys. **111**, 1815 (1999).
[43] A. K. Jameson and C. J. Jameson, Chem. Phys. Lett. **134**, 461 (1987).
[44] R. R. Gupta, *Diamagnetic Susceptibility*, Landolt-Börnstein, New Series, Group II, Vol. 16, Pt. B (Springer, New York, 1986).
[45] B. G. Pfrommer, F. Mauri, and S. G. Louie, J. Am. Chem. Soc. **122**, 123 (2000).